

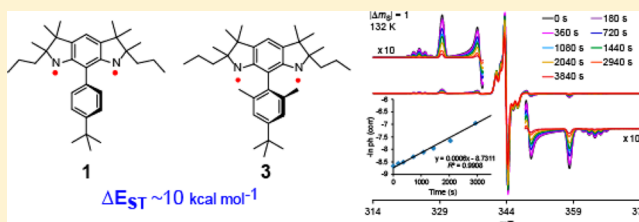
Aza-*m*-Xylylene Diradical with Increased Steric Protection of the Aminyl Radicals

Arnon Olankitwanit, Suchada Rajca, and Andrzej Rajca*

Department of Chemistry, University of Nebraska, Lincoln, Nebraska 68588-0304, United States

S Supporting Information

ABSTRACT: Aminyl diradical **3**, a derivative of aza-*m*-xylylene, is expected to be more stable than diradical **1**, due to increased steric protection of the radicals by additional methyl groups in the pendant group. Here we report synthesis and characterization of diradical **3**. The structure of diamine precursor **6** is characterized by high-field ¹H NMR spectroscopy in which the two diastereomers (*meso* and \pm pair) are distinguishable. In addition, correlation between the DFT-calculated and experimental ¹H and ¹³C NMR chemical shifts provides evidence in support of the diamine structure. Electrochemistry of the diamine is carried out to explore redox properties and stability of the corresponding aminium diradical dication. The ground state and ΔE_{ST} for **3** are established by statistical analyses of mean χT determined by EPR spectroscopy. Decay kinetics of aminyl diradical **3** indicates that the decay of **3** is faster than that of **1**, possibly due to intramolecular hydrogen atom abstraction from benzylic methyl groups in **3**, followed by intermolecular hydrogen atom abstraction from 2-MeTHF solvent.



INTRODUCTION

High-spin diradicals with large singlet–triplet energy gaps (ΔE_{ST}) that far exceed the thermal energy at room temperature ($\Delta E_{ST} \gg 0.6 \text{ kcal mol}^{-1}$) have great potential as building blocks for organic materials with novel magnetic properties.^{1–8} Organic radicals that are strongly paramagnetic at room temperature could impact development of organic paramagnetic contrast agents for magnetic resonance imaging (MRI)^{9,10} and relaxation enhancement NMR spectroscopy.¹¹ Purely organic magnets with magnetic ordering near room temperature are among the most fascinating targets which remain elusive.^{5,12,13} The promising pathway toward practical applications of these materials relies on the development of high-spin diradicals with $\Delta E_{ST} \gg 0.6 \text{ kcal mol}^{-1}$ that are persistent at room temperature.^{3a,6–8}

We recently reported aminyl diradicals **1** and **2**—derivatives of aza-*m*-xylylene (Figure 1) which possess triplet ground states with $\Delta E_{ST} \approx 10 \text{ kcal mol}^{-1}$.^{14–16} These diradicals are persistent at room temperature, with half-life values on the

order of minutes. Compared to the well-known reactive intermediate *m*-xylylene diradical ($\Delta E_{ST} \approx 10 \text{ kcal mol}^{-1}$),¹⁷ which is observable in solution at room temperature for hundreds of nanoseconds,¹⁸ these aminyl diradicals are notable advances in high-spin organic molecules. The next step is to improve the persistence of these diradicals while maintaining their triplet ground state with large values of $\Delta E_{ST} \approx 10 \text{ kcal mol}^{-1}$. The straightforward strategy is to increase steric protection of the aminyl diradicals, such as in diradicals **3** and **4** (Figure 2) with additional methyl and *tert*-butyl groups in the pendant group.

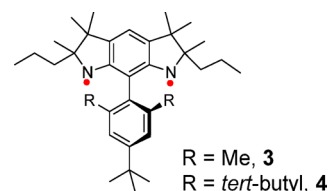


Figure 2. Sterically protected aminyl diradicals.

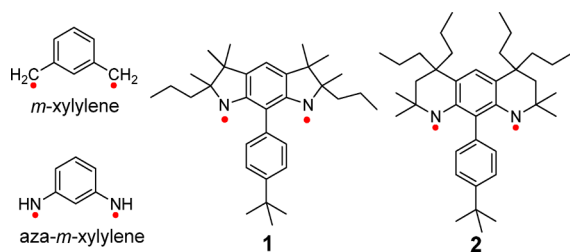


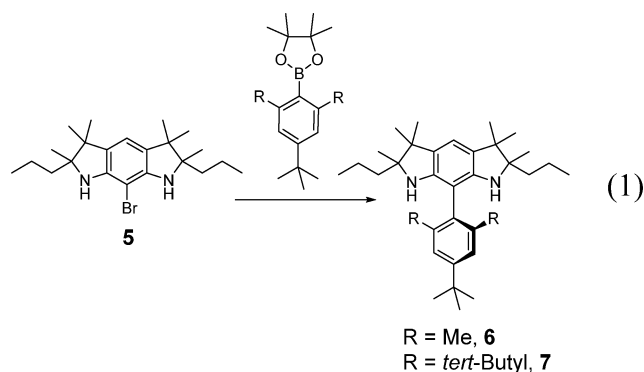
Figure 1. *m*-Xylylene, aza-*m*-xylylene, and aminyl diradicals **1** and **2**.

Diamines **6** and **7** (eq 1), precursors to diradicals **3** and **4** (Figure 2), could be accessible from the previously prepared bromoamine **5** via the Suzuki-Miyaura cross-coupling with pinacolboronate, similar to the established synthetic pathway to diamine precursor to aminyl diradical **1**.¹⁴

These are attractive targets for the first step, laying the groundwork for further development of aza-*m*-xylylene with

Received: February 23, 2015

Published: April 22, 2015



improved stability. As we worked on the synthesis, we could obtain diamine **6** but we were disappointed that our attempts to synthesize diamine **7**, by the Suzuki-Miyaura cross-coupling between **5** and its corresponding pinacolboronate, were not successful. In addition, we were surprised to find that the sterically shielded diradicals **3** decay more rapidly than **1**.

Here we report synthesis and characterization of diamine **6** and the corresponding aminyl diradical **3**. Structure of diamine **6** is characterized by high-field ^1H NMR spectroscopy in which the two diastereomers (*meso*-**6** and \pm pair-**6**) are distinguishable. In addition, correlation between the DFT-calculated and experimental ^1H and ^{13}C NMR chemical shifts provides evidence in support of the diamine **6** structure. Electrochemistry of diamine **6** is carried out to explore redox properties and stability of the corresponding aminium diradical dications. The ground state and ΔE_{ST} for **3** are established by statistical analyses of mean χT determined by EPR spectroscopy,¹⁵ and decay kinetics of aminyl diradical **3** is investigated by EPR spectroscopy.

RESULTS AND DISCUSSION

Synthesis of Diamine 6—Precursor to Diradical 3.

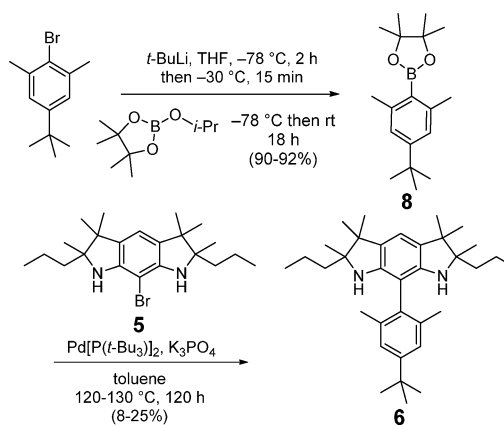
The pinacolboronate **8** was prepared by adopting a known procedure starting with Br/Li exchange using *t*-BuLi (2.1 equiv) in THF at $-78\text{ }^\circ\text{C}$ of 1-bromo-2,6-dimethyl-4-*tert*-butylbenzene, followed by borylation reaction using 2-isopropoxy-4,4,5,5-tetramethyl-1,3,2-dioxaborolane.¹⁹

We first attempted the Suzuki-Miyaura cross-coupling of **8** with bromodiamine **5** using tetrakis(triphenylphosphine)-palladium and the conditions employed to prepare the diamine precursor to diradical **1**.¹⁴ However, the reaction failed to yield the target diamine **6**. We then tried using $\text{Pd}_2(\text{dba})_3$ and a highly reactive phosphine ligand, Sphos,²⁰ which also failed to provide diamine **6**. Finally, we modified the conditions of Fu and co-workers, who employed the $\text{Pd}_2(\text{dba})_3/\text{P}(t\text{-Bu})_3/\text{KF}$ catalytic system,²¹ by using the $\text{Pd}[\text{P}(t\text{-Bu}_3)]_2/\text{K}_3\text{PO}_4$ catalytic system and we obtained target diamine **6** in low yield (Scheme 1).

In our efforts to prepare even more sterically shielded diamine **7** with *tert*-butyl groups in the pendant, we could obtain the corresponding pinacol boronate from 1-bromo-2,4,6-tri-*tert*-butylbenzene by employing a procedure analogous to that for **8**, but attempts at the Suzuki-Miyaura cross-coupling, using the $\text{Pd}[\text{P}(t\text{-Bu}_3)]_2/\text{K}_3\text{PO}_4$ catalytic system, did not provide diamine **7** (Supporting Information).

NMR Spectroscopy of Diamine 6. The structure of diamine **6** is characterized by high-field ^1H NMR spectroscopy. As expected, the two diastereomers (*meso*-**6** and \pm pair-**6**), originating from two diastereomers of bromodiamine **5**,

Scheme 1. Synthesis of Diamine 6—Precursor to Diradical 3



are distinguishable (Figure 3). Moreover, it appears that the rotation of the pendant aryl ring is slow on the 700 MHz ^1H NMR time scale at room temperature.

The slow rotation of the pendant group is evidenced by the observation of three singlet peaks for both the methyl groups (6H_d at $\delta = 2.053, 2.043,$ and 2.033 ppm) and the aromatic protons (2H_a at $\delta = 7.089, 7.083,$ and 7.078 ppm).²² The center singlet peaks correspond to \pm pair-**6** because two methyl groups (H_d) or two aromatic protons (H_a) are expected to be homotopic (related by a rotation about a C_2 -axis). The outer two singlet peaks correspond to *meso*-**6** because both the methyl groups and aromatic protons are expected to be diastereotopic. These findings also indicate that the ratio of the diastereomers, *meso*-to \pm pair, is about 2, which is consistent with the analysis of the aliphatic region of the ^1H NMR spectrum in Figure 3.

A broad singlet peak at $\delta = 2.931$ ppm (2H_c) in chloroform-*d* is assigned to the N-H group. This assignment was confirmed by a cross-peak between ^1H at $\delta = 3.216$ ppm (2H_c) and ^{15}N in ^1H - ^{15}N HSQC spectra in acetone-*d*₆; the ^{15}N NMR chemical shift is $\delta = -288.2$ ppm (Figure S5, Supporting Information). Additional evidence for the N-H group is obtained from a complete H/D exchange of the singlet at $\delta = 3.051$ ppm (2H_c) in benzene-*d*₆.

^1H and ^{13}C NMR spectra of **6** in acetone-*d*₆ or chloroform-*d* are obtained using standard 2D NMR spectroscopy, including ^1H - ^{13}C HSQC, ^1H - ^{13}C HMBIC, ^1H - ^1H NOESY, and ^1H - ^{15}N HSQC (Figures S1 and S2, S5–S9, SI), to assign the chemical shifts. We obtain the correlation between the DFT-calculated and experimental ^1H and ^{13}C NMR chemical shifts.

Geometry of **6a**, a simplified structure for **6**, in which the *n*-propyl groups are replaced with methyl groups (Figure 4), and tetramethylsilane are optimized at the B3LYP/6-31G(d,p) level of theory and confirmed as minima by vibrational analyses.²³ Using these DFT-optimized geometries, ^1H and ^{13}C NMR isotropic shieldings for **6a** and tetramethylsilane are computed at the GIAO/B3LYP/6-31G(d,p) level of theory with the IEF-PCM-UFF solvent model for acetone or chloroform (Gaussian 09),^{23–25} to provide calculated ^1H and ^{13}C NMR chemical shifts $\delta_{\text{DFT}}(^1\text{H})$ and $\delta_{\text{DFT}}(^{13}\text{C})$ for direct comparison with the experimental NMR spectra of **6** in acetone-*d*₆ and chloroform-*d*.^{26,27} For reference, the data for previously studied diamines precursors to diradicals **1** and model diradical **1a** are presented in the Supporting

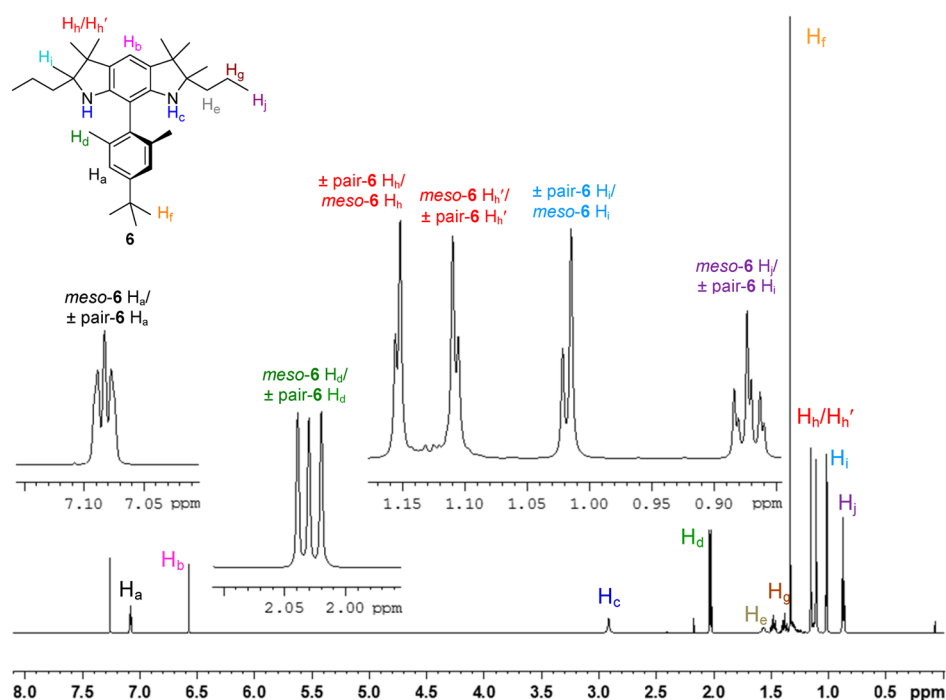


Figure 3. ^1H NMR (700 MHz, chloroform- d) spectrum of diamine **6**. Note that the methyl groups, labeled H_h and H_h' , are diastereotopic in both diastereomers of **6**.

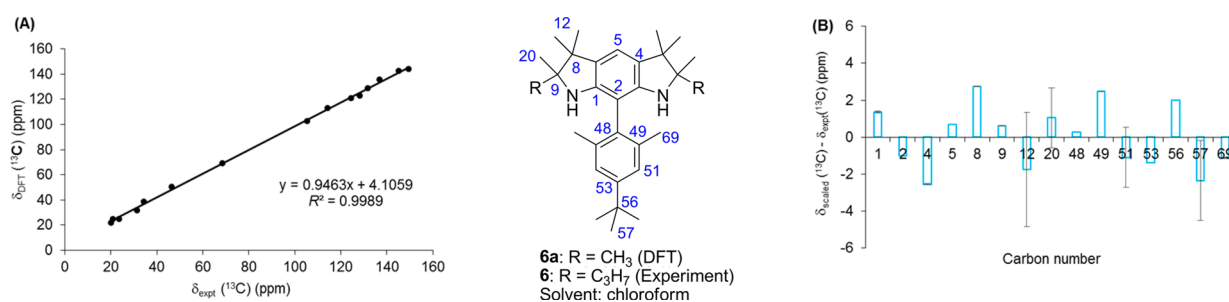


Figure 4. (A) Correlations between calculated (δ_{DFT}) and experimental (δ_{expt}) ^{13}C NMR chemical shifts for **6a** and **6**, respectively. Solid lines are the best fit to $\delta_{\text{DFT}} = a + b \delta_{\text{expt}}$. (B) Difference between scaled ($\delta_{\text{scaled}} = (\delta_{\text{DFT}} - a)/b$) and experimental (δ_{expt}) ^{13}C NMR chemical shifts; error bars correspond to the standard deviation of chemical shifts calculated for carbon atoms that are magnetically equivalent by symmetry and rotation. Statistical parameters are summarized in Table 1. Further details are reported in Figures S3 and S4 and Table S1 (Supporting Information).

Information.¹⁵ Correlations between DFT-computed and experimental ^{13}C NMR chemical shifts give correlation coefficients (R^2) that are expected for correctly assigned structures of small-sized organic molecules (Figure 4 and Table 1).^{25,28}

Table 1. Statistical Parameters for the Correlations of ^{13}C and ^1H NMR Chemical Shifts.^a

	a	b	R^2	MaxErr	CMAE (n)
6/6a (^{13}C)	4.1059	0.9463	0.9989	2.76	1.495 (15)
6/6a (^1H)	-0.0490	1.0378	0.9934 ^b	0.47	0.134 (7)

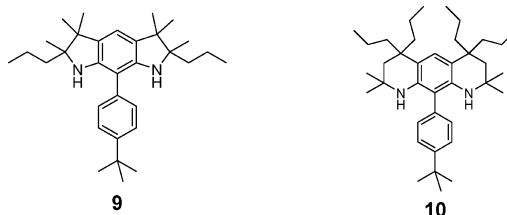
^a a and b are the intercept and slope of the linear fit to $\delta_{\text{DFT}} = a + b \delta_{\text{expt}}$, and R^2 is its correlation coefficient. MaxErr is the maximum corrected absolute error with respect to the linear fit ($|\delta_{\text{scaled}} - \delta_{\text{expt}}|$). CMAE is the corrected mean absolute error for n chemical shifts ($\sum |\delta_{\text{scaled}} - \delta_{\text{expt}}|/n$). ^bIf the NH group is taken out of the correlation, the R^2 improves to 0.9996.

The relationship between computed and experimental NMR chemical shifts is further illustrated by applying the correlations to scale linearly $\delta_{\text{DFT}}(^{13}\text{C})$, to provide $\delta_{\text{scaled}}(^{13}\text{C})$, and then by plots of the differences between the scaled and experimental NMR chemical shifts for each distinct carbon atom in the structure (Figures 4).^{25–27} These plots confirm the good agreement between the theory and experiment, and specifically the low values of statistical parameters for ^{13}C NMR chemical shifts such as MaxErr and CMAE in Table 1, as expected for correctly assigned structures.

Similar analyses of the relationship between computed and experimental ^1H NMR chemical shifts are summarized in Table 1 and illustrated in the Supporting Information (Figures S3 and S4).

The DFT-computed ^{15}N NMR chemical shift for **6a** is $\delta \approx -288$ ppm, which is within 1 ppm of the experimental value for **6** and within the typical range for NH groups in similar diamines (Table S2, Supporting Information).^{14,15}

Electrochemistry of Diamine 6. Redox properties of diamine **6** are investigated and compared to the analogous

Table 2. Structures of Diamines **9** and **10**, and Oxidation Potentials of Diamines^{a,b}

compound	oxidation potentials	CV $E_{1/2}^{\text{ox}}$ (V)	SWV E_p^{ox} (V)	E_{HOMO} (eV) ^d
6	$E^{+/0}$	0.310 ± 0.003 (8)	0.302 ± 0.002 (6)	-4.7
	$E^{2+/+}$	1.450 ± 0.003^c (3)	-	
9	$E^{+/0}$	0.322 ± 0.002 (4)	0.320 ± 0.001 (6)	-4.7
	$E^{2+/+}$	1.410 ± 0.015^c (5)	-	
10	$E^{+/0}$	0.459 ± 0.007 (6)	0.426 ± 0.002 (4)	-4.8

^aFurther details are in Figures S10–S13, Supporting Information. ^bPotentials (vs SCE) from CV and SWV reported as arithmetic mean \pm standard deviation (n), where n is the number of voltammograms. For potential determinations, the voltammograms were recorded with scan rates of 50–200 for **6**, 50–500 for **9**, and 100–200 mV s^{-1} for **10** (and SWV, with frequency of 10 Hz) in 0.1 M $[n\text{-Bu}_4\text{N}]^+[\text{PF}_6]^-$ in dichloromethane, using 100 μm Pt-disk as working electrode. The potentials are calibrated with decamethylferrocene (Cp^*Fe) as the internal standard (-0.130 V vs SCE for $\text{Cp}^*\text{Fe}^{+/0}$ in dichloromethane).²⁹ ^cThe second oxidation potential was approximately estimated. ^dCalculated using the empirical relationship $E_{\text{HOMO}} = -(E_{\text{onset}}^{\text{ox}} + 4.4)$.^{30,31}

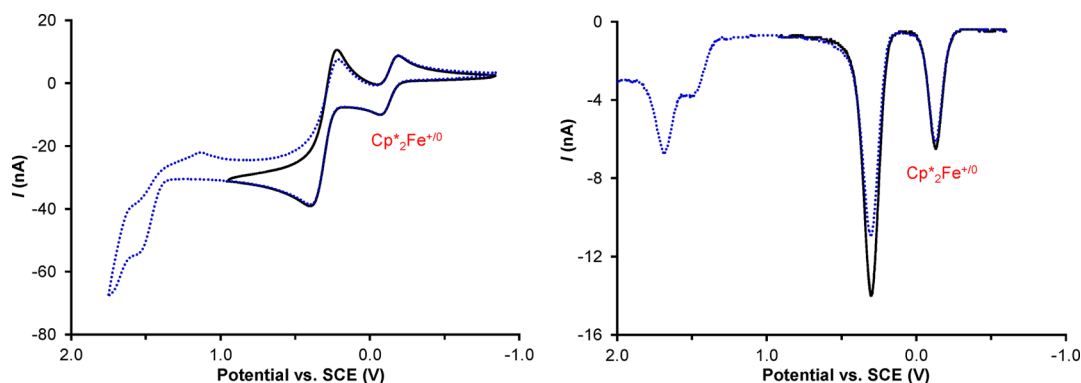


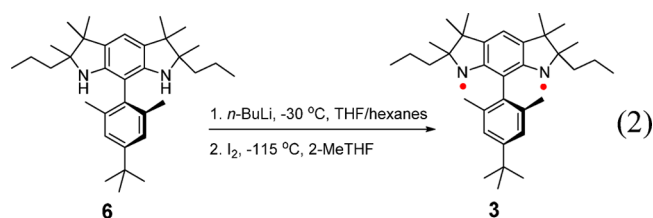
Figure 5. Cyclic voltammograms (CV, 200 mV s^{-1}) and square wave voltammograms (SWV, frequency 10 Hz, pulse height 25 mV) for diamine **6** in 0.1 M $[n\text{-Bu}_4\text{N}]^+[\text{PF}_6]^-$ in dichloromethane, and internally referenced to $\text{Cp}^*\text{Fe}^{+/0}$ (-0.130 V vs SCE).²⁹ Voltammograms for **9** and **10**, including decamethylferrocene reference, are shown in Figures S11 and S12 (Supporting Information). Oxidation potentials are summarized in Table 2.

diamines **9** and **10**. Cyclic voltammograms (CV) and square wave voltammograms (SWV) for **6** and **9** indicate that reversible oxidations to the corresponding aminium radical cations, with the first oxidation potential, $E^{1+/0} = 0.30\text{--}0.32$ V (Table 2 and Figure 5). Diamine **10** possesses considerably higher $E^{1+/0} = 0.43\text{--}0.46$ V that is not completely reversible under the experimental conditions (Table 2, Figure S12, Supporting Information). The onsets of oxidation suggest that the HOMO energy is about -4.7 eV in **6** and **9**, and about -4.8 eV in **10** (Table 2).^{30,31} These energies are slightly higher than the HOMO energy of -4.9 eV found in diazapentacene-based diaryl diamine.²⁶

However, oxidation of **6**, **9**, and **10** to the corresponding diradical dication is not reversible, with the estimated second oxidation potential, $E^{2+/+} \approx 1.41\text{--}1.45$ V for both **6** and **9**. These potentials are much higher than $E^{2+/+} \approx 1.16$ V in the diazapentacene-based diaryl diamine.²⁶ These results suggest that the corresponding aminium diradical dication is not likely to be persistent at room temperature.

Preparation of Aminyl Diradical 3. Diradical **3** was obtained according to the procedure for preparation of the analogous aminyl diradicals **1** and **2**.^{14,15} Diamine **6** (ca. 1 mg) was treated with $n\text{-BuLi}$ (2.2 equiv) in tetrahydrofuran/

hexanes (THF/hexanes) at -30 °C, and then after solvent exchange to 2-methyltetrahydrofuran (2-MeTHF), the resultant dianion was oxidized with iodine at -115 °C. The iodine was vacuum transferred in portions into the EPR sample tube (eq 2).



The EPR spectra of 8.0 mM aminyl diradical **3** in 2-MeTHF matrix at 132 K showed six symmetrically disposed side peaks corresponding to triplet state of diradical ($|\Delta m_s| = 1$). Also, the forbidden half-field transition ($|\Delta m_s| = 2$), which is characteristic of the triplet state, was observed. The center peak was assigned to a monoradical byproduct.

The EPR spectrum of **3** can be simulated using the zero-field splitting (zfs) parameters, $|D/hc| = 18.4 \times 10^{-3} \text{ cm}^{-1}$, $|E/hc| = 2.77 \times 10^{-3} \text{ cm}^{-1}$. Pentuplets of the outermost peaks are

reproduced with splitting of $|A_{zz}/2hc| = 1.20 \times 10^{-3} \text{ cm}^{-1}$ from two equivalent ^{14}N nuclei. These EPR spectral parameters are similar to those for diradicals **1** and **2** (Figure 6 and Table 3),^{14,15} and are quite distinct from those for planar $S = 1$ nitroxide diradicals.³²

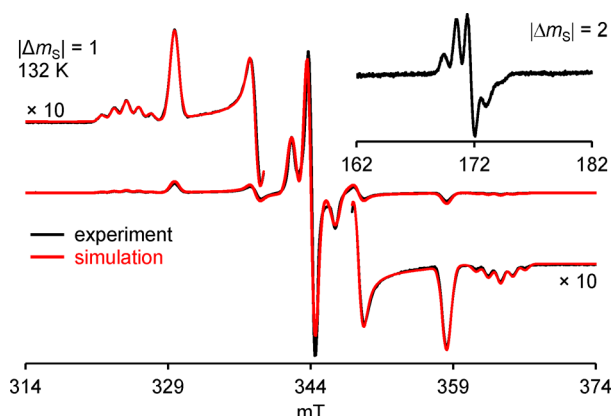


Figure 6. EPR (X-Band, $\nu = 9.6451 \text{ GHz}$) spectrum of aminyl diradical **3** in 2-MeTHF at 132 K; inset plot: $|\Delta m_s| = 2$ region, $\nu = 9.6449 \text{ GHz}$. The simulation parameters for the $S = 1$ state are $|D/hc| = 18.4 \times 10^{-3} \text{ cm}^{-1}$, $|E/hc| = 2.77 \times 10^{-3} \text{ cm}^{-1}$, $|A_{zz}/2hc| = 1.20 \times 10^{-3} \text{ cm}^{-1}$, $g_x = 2.0045$, $g_y = 2.0027$, $g_z = 2.0014$, Gaussian line ($L_x = 0.84$, $L_y = 0.94$, $L_z = 0.76 \text{ mT}$). The center lines correspond to an $S = 1/2$ (monoradical) byproduct simulated with the identical g -values, $|A_{zz}/hc| = 2.15 \times 10^{-3} \text{ cm}^{-1}$ and Gaussian line ($L_x = 0.8$, $L_y = 0.8$, $L_z = 0.9 \text{ mT}$). Further details may be found in Figures S14–S17 in the Supporting Information.

Decay Kinetics of Aminyl Diradical 3. The persistence of **3** in 2-MeTHF was investigated by EPR spectroscopy, analogously to **1** and **2**. A typical kinetic run is illustrated using a sample of 2.7 mM diradical **3** (Figure 7). We were surprised to discover that **3** already started to decay at 246 K according to the first order kinetics with a half-life, $\tau_{1/2} = 19.34 \pm 1.67 \text{ min}$ (mean \pm 95% confidence interval). For another sample of **3**, $\tau_{1/2} = 16.53 \pm 2.43 \text{ min}$ at 246 K was determined (Table S5, Supporting Information).

These findings are in contrast to no change of EPR signal for most studied samples of **1** and **2** at 246 K,^{15,33} thus implying that diradical **3** is much less persistent than **1** and **2**.

After annealing diradical **3** at room temperature with exclusion of light for 2–4 d, HR EI-MS of the crude reaction mixtures show diamine **6** as the predominant product (Figures S27C and S28C, Supporting Information). However, ^1H NMR spectra of the crude mixtures are complicated and TLC analyses show the presence of a significant amount of

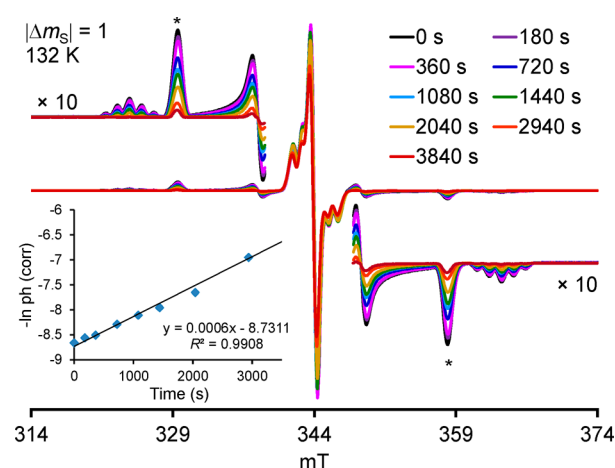


Figure 7. Decay kinetics for 2.7 mM diradical **3** in 2-MeTHF at 246 K: for the peaks at ~ 330 and 358 mT , asterisks indicate the peaks plotted in the inset plot as $-\ln \text{ph (corr)}$ vs Time, where “ph (corr)” corresponds to averaged peak heights, for which intensities were corrected with the nitroxide reference (1.0 mM TEMPONE). Further details may be found in Figures S18–S20 and Tables S5 and S6 in the Supporting Information.

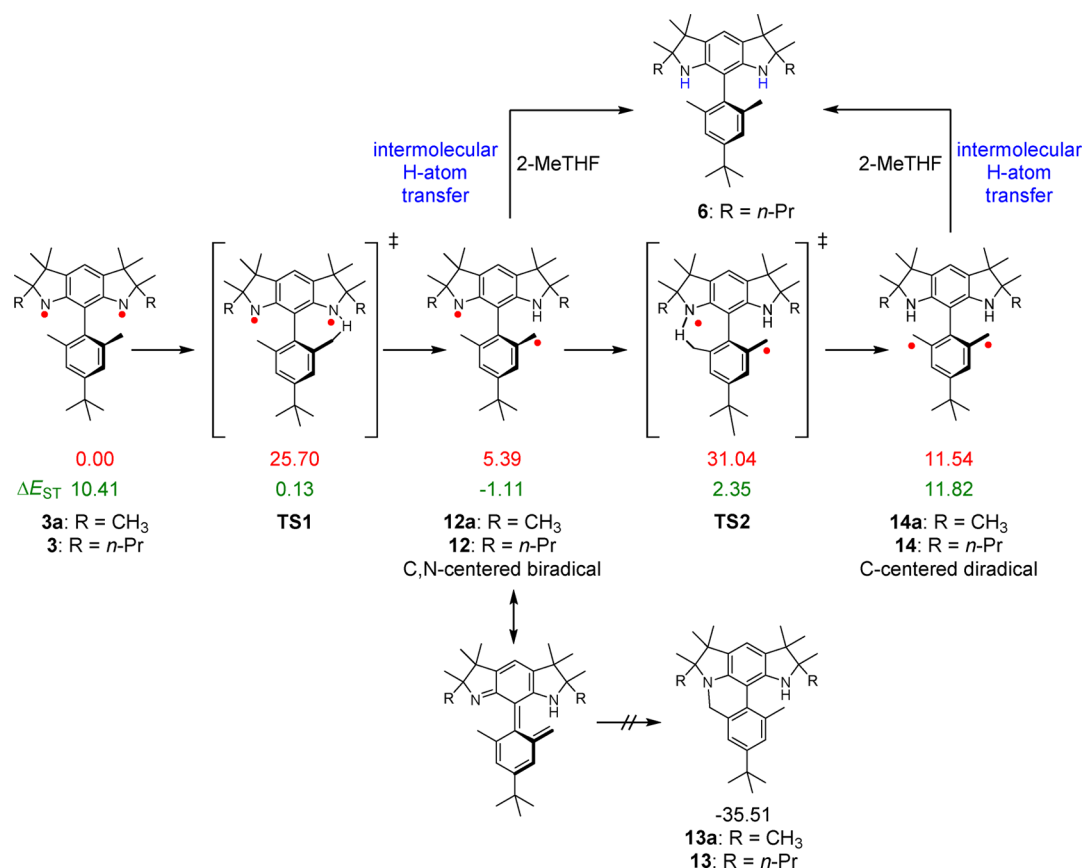
materials that are much more polar than diamine **6**. Filtration of the crude mixtures through silica gives diamine **6** corresponding to ~ 20 – 30% recovery (Figures S24 and S26). Conversion of aminyl diradical **3** to diamine **6** may take place via a hydrogen-atom abstraction mechanism because of low C–H bond dissociation energy, $\sim 92 \text{ kcal mol}^{-1}$, of solvent such as 2-MeTHF or THF,^{34–36} however, this would not explain why diradical **3** decays much more rapidly than **1**. We considered that diradical **3** may decay via an intramolecular hydrogen-atom abstraction mechanism involving benzylic methyl groups, which possess C–H bond dissociation energy of $\sim 90 \text{ kcal mol}^{-1}$.^{34,37} We computed such a reaction using the model diradical **3a** at the UB3LYP/6-31G(d,p) level of theory, which provided an activation energy of $\sim 26 \text{ kcal mol}^{-1}$ (Scheme 2, Table S9, Figures S22 and S23, Supporting Information).³⁶

The intramolecular hydrogen-atom abstraction at the benzylic methyl groups in **3a** would lead to C,N-centered biradical **12a**, which upon rotation of the pendant group could undergo ring closure to form **13a**. However, at low temperatures, such rotation of sterically hindered pendant in the biradical is not likely. Indeed, the ring-closure product **13**, which is two m/z units below the m/z corresponding for diamine **6**, is not observed in HR EI-MS of the crude reaction mixtures. We postulate that the biradical **12**, which is expected to be a highly reactive intermediate, abstracts hydrogen atoms

Table 3. Summary of Experimental EPR Spectra for Aminyl Diradicals in 2-MeTHF at 132–133 K and Computed EPR Spectra at the B3LYP/EPR-II Level Using ORCA^a

diradical	conc. ^b (mM)	ν (GHz)	$ D/hc $ (10^{-3} cm^{-1})	$ E/hc $ (10^{-3} cm^{-1})	$ A_{zz}/2hc $ (10^{-3} cm^{-1})	g_x	g_y	g_z	g	calculations		
										$ D/hc $ (10^{-3} cm^{-1})	$ E/hc $ (10^{-3} cm^{-1})	$ A_{zz}/2hc $ (10^{-3} cm^{-1})
1 ^c	9	9.4780	17.49	3.60	1.13	2.0046	2.0030	2.0019	2.0032	34.4	0.02	1.13
2 ^d	5	9.6415	17.94	1.42	1.08	2.0050	2.0031	2.0018	2.0033	35.9	0.80	1.16
3	8	9.6451	18.40	2.77	1.20	2.0045	2.0027	2.0014	2.0029	36.0	1.51	1.21

^aFurther details may be found in Tables S3, S4, and S10 in the Supporting Information. ^bConcentration based on the mass of precursor diamines for diradicals **1**, **2**, and **3** and volume of the solvent. ^cref 14. ^dref 15.

Scheme 2. Plausible Pathways for the Decay of Aminyl Diradical 3^a

^aThe B3LYP/6-31G(d,p)//B3LYP/6-31G(d,p) relative energies and singlet–triplet energy gaps after ZPVE correction for simplified structures.

Table 4. Statistical Analyses of χT for Diradical 3

	sample 1			sample 2				
	χT_{EPR}	χT_{Int} 2J/k (K)			χT_{EPR}	χT_{Int} 2J/k (K)		
		0	164	113		0	76	49
	0.535289134	0.485616492	0.512499962	0.507126438	0.517148814	0.494986482	0.512946671	0.507577135
	0.528758434	0.489912267	0.518147501	0.512494059	0.530555348	0.498237069	0.516823233	0.511262718
	0.535241081	0.487645638	0.515164597	0.509659577	0.531260391	0.494407715	0.512257249	0.50692145
	0.514202611	0.486830753	0.514093856	0.508641798	0.530431878	0.497079739	0.515442159	0.509949931
	0.515791691	0.487023872	0.51434753	0.50888294	0.533451016	0.495070906	0.513047257	0.507672793
	0.518805148	0.486049864	0.513068603	0.507667103	0.50915416	0.499957961	0.518878612	0.51321596
n	6	6	6	6	6	6	6	6
Mean	0.52468135	0.487179814	0.514553675	0.509078652	0.525333601	0.496623312	0.514899197	0.509433331
Stdev	0.009633435	0.001519882	0.001998295	0.001899223	0.009828971	0.002187714	0.002609766	0.00248098
SEM	0.003932833	0.000620489	0.000815801	0.000775354	0.004012661	0.000893131	0.001065433	0.001012856
P		0.000174666	0.049309058	0.00993991		0.000626216	0.047748761	0.009630655

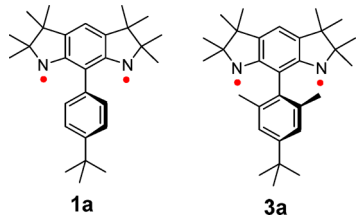
from 2-MeTHF to provide diamine 6.^{35,36} Alternatively, 12 might undergo intramolecular hydrogen abstraction at the other benzylic position to give rise to C-centered diradical 14, which would then abstract hydrogen atoms from 2-MeTHF to provide diamine 6.^{35,36} The computed activation energy for the reaction of 12a to 14a is 24.5 kcal mol⁻¹ on the triplet state potential energy surface (Scheme 2). In addition, biradical 12 and diradical 14 could undergo various other transformations, including dimerization/oligomerization at their sterically less encumbered benzylic radical positions, giving rise to polar compounds detected by TLC.

Determination of the Ground State and ΔE_{ST} for Diradical 3: Statistical Analyses of Mean χT Determined by EPR Spectroscopy. Because of the relatively low content of diradical 3 (~20–40%) in the samples, which precludes reliable determination of the ground state and lower limit of ΔE_{ST} by SQUID magnetometry,¹⁴ we used our recently developed approach based upon statistical analyses of mean χT measured by EPR spectroscopy.¹⁵ The estimated χT as a function of ΔE_{ST} (χT_{Int}) is obtained from double integrated peak intensities of diradical and monoradical in the sample, and the total χT (χT_{EPR}) is measured using a spin counting standard.

For a given sample of **3** in 2-MeTHF, the difference between the mean χT of each of the χT_{Int} and χT_{EPR} data sets is tested for statistical significance, to determine the triplet ground state and ΔE_{ST} . The test is carried out using a two-tailed two-sample *t* test for means with unequal variances (Welch variant of *t* test), to compare the mean χT_{Int} with the mean χT_{EPR} . This comparison identifies the differences between the means that would be significant at the probability *P*, e.g., $P < 0.05$ and $P < 0.01$. For example, the difference between mean χT_{EPR} and χT_{Int} ($2J/k = 0$ K) is very significant with a probability $P = (2-6) \times 10^{-4}$, indicating unequivocally a triplet ground state (Table 4). The difference is significant at a probability $P < 0.05$ when $2J/k = 164$ or 76 K; at a more statistically significant probability, $P < 0.01$, smaller values of $2J/k = 113$ or 49 K are obtained. These results establish that **3** possesses triplet ground state with $\Delta E_{\text{ST}} > 0.3$ kcal mol⁻¹.

DFT Computation of Singlet–Triplet Energy Gaps and EPR Tensors. The simplified structures of aminyl diradicals **1** and **3**, i.e., **1a**^{14,15} and **3a** (Table 5), were studied

Table 5. DFT-Computed Singlet-Triplet Energy Gaps (ΔE_{ST}).^a



diradical	BS-DFT+ZPVE level	ΔE_{UHF} (kcal mol ⁻¹)	ΔE_{ST} (kcal mol ⁻¹)
1a	UB3LYP/6-31G(d) ^b	6.12	11.58
	UB3LYP/6-311+G(d,p) ^b	5.86	11.03
	UM06-2X/6-31G(d) ^b	6.25	11.94
3a	UB3LYP/6-31G(d)	5.60	10.42
	UB3LYP/6-311+G(d,p)	5.36	9.92
	UM06-2X/6-31G(d)	5.64	10.69

^aOptimized geometries and zero-point vibrational energy correction for the triplet and broken-symmetry singlet. Further details may be found in Table S8, Supporting Information. ^brefs 15 and 16.

at the UB3LYP/6-31G(d)+ZPVE, UB3LYP/6-311+G(d,p)+ZPVE, and UM06-2X/6-31G(d)+ZPVE levels of theory. Geometries were optimized for both triplet and broken-symmetry (BS) singlet states. Conformations of the lateral rings of the fused tricyclic moieties are oriented “anti”, i.e., in **3a**, the fused tricyclic moiety has an approximate *C*₂ point group of symmetry.

The ΔE_{ST} may be estimated using the energy difference between ground state triplet and BS singlet (ΔE_{UHF}) and the correction for spin contamination (eq 3).^{38–40}

$$\Delta E_{\text{ST}} = \Delta E_{\text{UHF}}[\langle S_T^2 \rangle / (\langle S_T^2 \rangle - \langle S_{\text{BS-S}}^2 \rangle)] \quad (3)$$

Diradical **1a** and diradical **3a** possess similar $\Delta E_{\text{ST}} \approx 10$ – 12 kcal mol⁻¹, as expected, because the spin density in both diradicals is predominantly confined to the aza-*m*-phenylene moiety (Figure 8). Most likely, our BS-DFT-computed values of ΔE_{ST} are overestimated;^{41–44} Barone and co-workers’ computation of **1a** at a much higher level of theory (DDCI) provided $\Delta E_{\text{ST}} \approx 9.6$ kcal mol⁻¹,¹⁶ which is about 2 kcal mol⁻¹ below the BS-DFT results in Table 5.

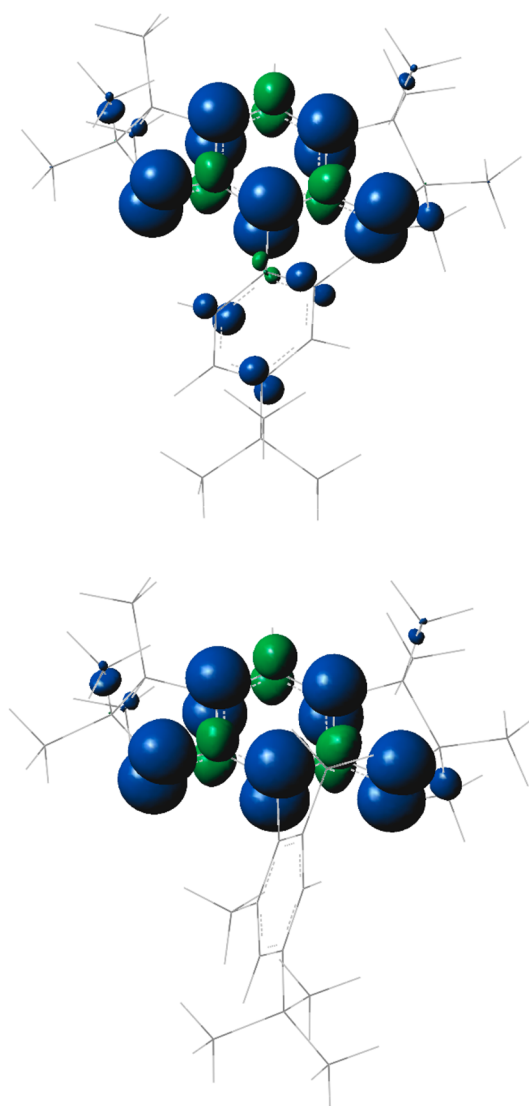


Figure 8. Spin density maps for the triplet ground state of diradicals **1a** (top) and **3a** (bottom) at the UB3LYP/EPR-III//UB3LYP/6-311+G(d,p) level of theory. Positive (blue) and negative (green) spin densities are shown at the isodensity level of 0.006 electron/Bohr.³

Calculations of EPR D-tensor and ¹⁴N A-tensors at the B3LYP/EPR-II//UB3LYP/6-311+G(d,p) level were carried out using ORCA,^{45,46} analogously to the previously reported computations of **1a** (Table S10, Supporting Information).¹⁴ The B3LYP/EPR-II-computed EPR spectra of **3a** provide the correct orientation of the D-tensor (and thus, the positive sign of *D*); in particular, the outermost lines (*Z*-lines) are split into pentuplets with the splitting of $A_{\text{ZZ}}/2hc$ showing excellent agreement between the theory and experiment for the ¹⁴N-hyperfine coupling of two equivalent nitrogens (Table 3). However, as in **1a** and other planar aminyl diradicals, the calculated value of the zero-field splitting parameter $D = 36.0 \times 10^{-3}$ cm⁻¹ in **3a** is overestimated by a factor of about 2.^{7,14,15}

3. CONCLUSION

Aminyl diradical **3** possesses triplet ground state with $\Delta E_{\text{ST}} > 0.3$ kcal mol⁻¹, as determined by the statistical analysis of its EPR spectra. This lower limit for experimental ΔE_{ST} can be

compared to the DFT-computed energy gap of 10 kcal mol⁻¹. In spite of increased steric protection of aminyl radicals, diradical **3** is less persistent in 2-MeTHF (half-life of ~20 min at 246 K), compared to diradical **1** (half-life of 10 min at 295 K). The faster decay of **3** is possibly due to intramolecular hydrogen atom abstraction from benzylic methyl groups, which may be then followed by intermolecular hydrogen atom abstraction from 2-MeTHF solvent to provide diamine **6**.

EXPERIMENTAL SECTION

NMR and IR Spectroscopy, Mass Spectrometry, and Computations. NMR spectra (¹H, 400, 500, 600, and 700 MHz) were obtained using benzene-*d*₆, acetone-*d*₆, and chloroform-*d* (CDCl₃) as solvent. The 500 and 700 MHz instruments were equipped with a cryoprobe. The chemical shift references were as follows: (¹H) benzene-*d*₆, 7.15 ppm; (¹³C) benzene-*d*₆, 128.39 ppm (benzene-*d*₆); (¹H) acetone-*d*₆, 2.05 ppm; (¹³C) acetone-*d*₆, 29.92 ppm (acetone-*d*₆); (¹H) chloroform, 7.26 ppm; (¹³C) CDCl₃, 77.0 ppm (CDCl₃). Natural abundance ¹H–¹⁵N HSQC spectra were externally referenced to ¹⁵N₂-labeled urea (98+% ¹⁵N, 0.7 mg in 0.4 mL of acetone-*d*₆). The reported ¹⁵N chemical shifts were converted to the δ ¹⁵N (nitromethane) = 0 ppm scale,⁴⁷ using the relation: δ ¹⁵N (urea) = δ ¹⁵N (nitromethane) + 304.7 ppm.⁴⁸

IR spectra were obtained using an instrument equipped with an ATR sampling accessory.

DFT computations were carried out using an 8-CPU workstation running Gaussian 09.²³ All optimized geometries had RMS forces in Cartesian coordinates of less than 1.2 × 10⁻⁵ a.u. Except for transition states for the intramolecular hydrogen-atom transfer, all reported computed structures are minima on the gas phase potential energy surface, as determined by vibrational analyses (Tables S4, Supporting Information).

Electrochemistry. Cyclic voltammetry and square wave voltammetry data were obtained in a glovebag under argon atmosphere using a commercial potentiostat/galvanostat. About 1 mg of diamine **6**, **7**, or **8** was dissolved in the supporting electrolyte solution (2.4 mL), 0.1 M tetrabutylammonium hexafluorophosphate (*n*-Bu₄NPF₆) in anhydrous DCM, and then transferred to a custom-made cell equipped with quasi-reference (Ag-wire), counter (Pt-foil), and working (100-μm Pt-disk) electrodes. The redox potentials were referenced to SCE using an internal decamethylferrocene (–0.130 V vs SCE for Cp*₂Fe/Cp*₂Fe⁺ in CH₂Cl₂).²⁹ For each compound, plots of peak current vs square root of scan rate (50–500 or 20–500 mV/s) in cyclic voltammetry were linear. A detailed description of the voltammetry may be found in the Supporting Information.

Synthesis. Standard techniques for synthesis under inert atmosphere (argon or nitrogen), using custom-made Schlenk glassware, custom-made double manifold high vacuum lines, and argon-filled Vacuum Atmospheres gloveboxes, were employed. Chromatographic separations were carried out using normal phase silica gel; for separations of diamine **6**, silica gel was deactivated by treatment with 3% of triethylamine in pentane or hexane.⁴⁹

Boronate 8. 1-Bromo-4-*tert*-butyl-2,6-dimethylbenzene (0.101 g, 0.418 mmol, 1 equiv) was transferred into a Schlenk vessel and evacuated under high vacuum for 10 min. Freshly distilled THF (1.5 mL) was added into the reaction vessel. After stirring at room temperature for 5 min, the reaction was cooled to –78 °C for 15 min. *t*-BuLi (1.59 M, 0.55 mL, 0.879 mmol, 2.1 equiv) was added dropwise to the Schlenk vessel. The reaction mixture was stirred at –78 °C for 2 h to produce milky solution. The reaction was then stirred at –30 °C for 15 min, then was cooled down to –78 °C for 15 min. 2-Isopropoxy-4,4,5,5-tetramethyl-1,3,2-dioxaborolane (0.12 mL, 0.586 mmol, 1.4 equiv) was added to the reaction mixture. The reaction was stirred and allowed to warm up to room temperature slowly for overnight. After 18 h, the milky solution was worked up with a brine solution (2 mL). The crude mixture was extracted with diethyl ether (3 × 25 mL). The organic phase was combined, dried over MgSO₄, and evaporated *in vacuo* to give a white solid of the target product **4** (0.111 g, 92%). Mp 162–163 °C. *R*_f = 0.11

(pentane). ¹H NMR (400 MHz, chloroform-*d*): δ = 6.992 (s, 2H), 2.433 (s, 6H), 1.384 (s, 12H), 1.293 (s, 9H). ¹³C NMR (100 MHz, chloroform-*d*): δ = 152.2, 141.9, 123.7, 83.4, 34.3, 31.2, 24.9, 22.6. IR (cm⁻¹): 3052, 2962, 2864, 1605, 1373, 1335, 1301, 1265, 1139, 1061, 960, 857, 735. HRMS (EI), *m/z* ion type (%RA for *m/z* = 50–400): Calcd for ¹²C₁₈¹H₂₉¹⁶O₂¹¹B [M]⁺ 288.2261; Found 288.2270 (23%). Calcd for ¹²C₁₇¹H₂₆¹⁶O₂¹¹B [M-CH₃]⁺ 273.2026; Found 273.2016 (100%).

Diamine 6. Bromodiamine **5** (35.9 mg, 88.1 μmol) was transferred to a Schlenk vessel and evacuated under high vacuum for 3 h. Boronate **4** (76.2 mg, 264 μmol, 3 equiv) and anhydrous K₃PO₄ (93.5 mg, 441 μmol, 5 equiv) were charged into the Schlenk vessel under N₂ atmosphere. Pd[P(*t*-Bu)₃]₂ (36.0 mg, 70.5 μmol, 0.8 equiv) was added to the vessel in a glovebox under Ar atmosphere. Finally, toluene (1 mL) was added to the vessel by vacuum transfer. The reaction was stirred for 5 d at 130 °C, with exclusion of light. After cooling down to room temperature, the reaction mixture was diluted by chloroform and filtered through a Celite pad to provide the crude mixture. Column chromatography (3% deactivated silica, diethyl ether/pentane, 1:33, *R*_f = 0.79) provided the diamine **6** (10.9 mg, 25%) as a white solid. Mp 152–160 °C (dec, under air). ¹H NMR (500 MHz, benzene-*d*₆): δ = 7.377 (s, 2H), 6.894 (s, 1H), 3.048 (s, 2H, exch D₂O), 2.400 (t, *J* = 2.5 Hz, 6H), 1.408–0.739 (m, 8H), 1.310 (m, 6H), 1.275 (s, 6H), 1.256 (s, 9H), 0.893 (s, 3H), 0.886 (s, 3H), 0.707–0.669 (m, 6H). ¹H NMR (500 MHz, chloroform-*d*): δ = 7.095 (bs, 2H), 6.589 (s, 1H), 2.931 (bs, 2H), 2.053–33 (s, 6H), 1.547–1.275 (m, 8H), 1.343 (s, 9H), 1.165 (s, 6H), 1.121 (s, 6H), 1.030 (s, 6H), 0.883 (t, *J* = 7.0 Hz, 6H). ¹H NMR (500 MHz, acetone-*d*₆): δ = 7.165, 7.155, 7.144 (s, 2H, mixture of diastereomers), 6.698 (s, 1H), 3.216 (bs, 2H), 1.568–1.278 (m, 8H), 1.331 (s, 9H), 1.182, (s, 6H), 1.125 (s, 6H), 1.057 (s, 6H), 0.864 (t, *J* = 7.2 Hz, 6H). ¹H–¹⁵N HSQC (acetone-*d*₆): δ (¹⁵N) = –287.8 ppm. ¹³C NMR (100 MHz, chloroform-*d*): δ = 149.5, 145.0, 137.2, 136.8, 136.4, 131.7, 128.1, 124.66, 124.50, 124.33, 114.2, 105.3, 68.4, 46.4, 38.4, 34.3, 31.5, 23.89, 23.85, 23.5, 20.9, 20.04, 20.02, 19.99, 18.0, 14.9. IR (cm⁻¹): 3375, 2956, 2932, 2871, 1602, 1435, 1381, 1364, 1301, 1156, 1127, 868, 756. HRMS (EI), *m/z* ion type (%RA for *m/z* = 200–650): Calcd for ¹²C₃₄¹H₅₂¹⁴N₂ [M]⁺ 488.4131; Found 488.4131 (35%). Calcd for ¹²C₃₃¹H₄₉¹⁴N₂ [M-CH₃]⁺ 473.3896; Found 473.3866 (100%).

4,4,5,5-Tetramethyl-2-(2,4,6-tri-*tert*-butylphenyl)-1,3,2-dioxaborolane (pinacol 2,4,6-tri-*tert*-butylphenylboronate). 1-Bromo-2,4,6-tri-*tert*-butylbenzene (20.6 mg, 0.063 mmol, 1 equiv) was transferred into a Schlenk vessel and evacuated under high vacuum for 4 h. Freshly distilled THF (1 mL) was added into the reaction vessel. After stirring at room temperature for 5 min, the Schlenk vessel was cooled to –78 °C for 10 min. *t*-BuLi (1.68 M, 0.08 mL, 0.133 mmol, 2.1 equiv) was added dropwise to the reaction vessel. The reaction mixture was stirred at –78 °C for 1 h to produce a clear light yellow solution. The reaction was stirred at –30 °C for 20 min, then was cooled down to –78 °C for 10 min. 2-Isopropoxy-4,4,5,5-tetramethyl-1,3,2-dioxaborolane (0.02 mL, 0.089 mmol, 1.4 equiv) was added to the reaction mixture. The reaction was warmed up slowly to room temperature and stirred overnight. After 17 h, the milky solution was quenched by adding brine solution (2 mL) and extracted with diethyl ether (3 × 25 mL). The organic phase was combined, dried over Na₂SO₄, and evaporated *in vacuo* to give a crude product. The crude product was filtered through a short silica gel plug with pentane to 1% diethyl ether/pentane to obtain a white solid of the product (14.0 mg, 59% yield). Mp 175–176 °C. *R*_f = 0.19 (pentane). ¹H NMR (400 MHz, chloroform-*d*): δ = 7.373 (s, 2H), 1.486 (s, 18H), 1.466 (s, 12H), 1.313 (s, 9H). ¹³C NMR (100 MHz, chloroform-*d*): δ = 154.3, 149.6, 120.5, 83.9, 37.5, 34.9, 32.8, 31.3, 26.4. IR (cm⁻¹): 3001, 2954, 2909, 2869, 1603, 1363, 1317, 1293, 1140, 1057, 964, 857, 691. HRMS (EI), *m/z* ion type (%RA for *m/z* = 320–550): Calcd for ¹²C₂₄¹H₄₁¹⁶O₂¹¹B [M]⁺ 372.3200; Found 372.3203 (100%). Calcd for ¹²C₂₃¹H₃₈¹⁶O₂¹¹B [M-CH₃]⁺ 357.2965; Found 357.2970 (58%).

Attempted Synthesis of Diamine 7. Bromodiamine **5** (6.1 mg, 15.0 μmol) was transferred into a Schlenk tube and evacuated under

high vacuum for overnight. 4,4,5,5-Tetramethyl-2-(2,4,6-tri-*tert*-butylphenyl)-1,3,2-dioxaborolane (16.7 mg, 45.0 μmol , 3 equiv) and anhydrous K_3PO_4 (15.9 mg, 74.9 μmol , 5 equiv) were charged into the Schlenk vessel under N_2 atmosphere. $\text{Pd}[\text{P}(t\text{-Bu})_3]_2$ (6.1 mg, 12.0 μmol , 0.8 equiv) was added to the vessel in a glovebox. The reaction vessel was evacuated on high vacuum briefly and toluene (0.15 mL) was added to the reaction vessel by vacuum transfer. The reaction was stirred for 6 d (144 h) at 130 $^\circ\text{C}$ with exclusion of light. After cooling down to room temperature, the reaction mixture was diluted by chloroform and filtered through a Celite pad to provide the crude mixture. The crude mixture was separated by preparative TLC (3% deactivated silica, diethyl ether/pentane, 1:33) gave the starting boronate, debrominated diamine **5**, and trace amount of its dimer, **5-dimer**, as well as other unidentified byproducts (Figures S29 and S30, Supporting Information).

General Procedure for the Generation of 3. Diamine **6** (0.60–1.10 mg, 1.23–2.25 μmol) was placed in a custom-made Schlenk-EPR-tube (5 mm OD) and then it was placed under high vacuum (10^{-4} mTorr). The sample tube was heated at 70 $^\circ\text{C}$ overnight using a heating tape. After the heating tape around the sample area was removed, additional heating at 110 $^\circ\text{C}$ was applied to the remaining EPR tube overnight. These steps are critical for achieving appropriate environment for radical generation. THF (~ 0.1 mL, ~ 10 mm height) was added to the vessel by vacuum transfer, and then the solution was stirred for 30 min at -30 $^\circ\text{C}$. *n*-BuLi (0.15–0.27 M in hexane, 18–20 μL , 2.66–5.40 μmol , 2.1–2.4 equiv) was added at -30 to -50 $^\circ\text{C}$. The orange reaction mixture was stirred at -30 to -50 $^\circ\text{C}$ for 1–2 h, before the solvents were evaporated at -50 to -40 $^\circ\text{C}$, and then the reaction mixture was immersed in liquid nitrogen. 2-MeTHF (~ 0.1 mL) was added to the reaction mixture by vacuum transfer. After brief warming (under vacuum) to -80 or -100 $^\circ\text{C}$ to form a light orange solution, the reaction mixture was immersed in liquid nitrogen. Subsequently, iodine was vacuum transferred to the sample tube wall, just above the reaction mixture. Iodine was mixed into the reaction mixture at -115 $^\circ\text{C}$, and then the solution was stirred at -115 $^\circ\text{C}$ for 1 h. The resultant solution was stored in liquid nitrogen; EPR spectra were obtained at 132 or 133 K. Further experimental details are summarized in Table S11, Supporting Information.

General Procedure for the Measurements of χT for Statistical Analyses for 3. After obtaining the samples using the protocol described above, 2-MeTHF was added by vacuum transfer at liquid N_2 temperature, to obtain solution of ~ 4 –5 cm height in the EPR tube. The resultant solution was mixed by hand with a magnetic stir-bar (and external magnet) for additional 15–30 min at -115 $^\circ\text{C}$ before EPR spectra were taken at 132 K. Two EPR spectra of the sample and the nitroxide reference were obtained and their double integrations were averaged, separately for the sample and for the reference. Subsequently, the sample and the reference were annealed at -115 and 22 $^\circ\text{C}$, respectively. Following the annealing, the sample and the reference were frozen carefully with liquid N_2 to give a continuous (and bubble-free) block of 2-MeTHF glass, prior to placing the sample and the reference in the EPR cavity for another set of spectra. Overall, $n = 6$ of independent sets of spectra were obtained for each of the two samples of **3** and their references (Table 4).

General Procedure for Decay Kinetics Measurements for 3. After obtaining the dilute samples using the protocols described in the generation and statistical analyses of **3**, EPR spectra were taken at 132 K, following annealing of the samples at -27 $^\circ\text{C}$ (246 K). For EPR intensity reference, EPR spectra of TEMPONE (1 mM in 2-MeTHF) were obtained at 132 K.

■ ASSOCIATED CONTENT

■ Supporting Information

General procedures and materials, additional experimental details, computational data tables, and complete ref 23. The Supporting Information is available free of charge on the ACS Publications website at DOI: 10.1021/acs.joc.5b00421.

■ AUTHOR INFORMATION

Corresponding Author

*E-mail address: arajca1@unl.edu

Notes

The authors declare no competing financial interest.

■ ACKNOWLEDGMENTS

We thank the National Science Foundation for support of this research through grants CHE-1012578 and CHE-1362454, including the purchase of the electron paramagnetic resonance (EPR) spectrometer (DMR-0216788) used in this work.

■ REFERENCES

- (1) Abe, M. *Chem. Rev.* **2013**, *113*, 7011–7088.
- (2) Lineberger, W. C.; Borden, W. T. *Phys. Chem. Chem. Phys.* **2011**, *13*, 11792–11813.
- (3) (a) Gallagher, N.; Olankitwanit, A.; Rajca, A. *J. Org. Chem.* **2015**, *80*, 1291–1298. (b) Ratera, I.; Veciana, J. *Chem. Soc. Rev.* **2012**, *41*, 303–349. (c) Lahti, P. M. *Adv. Phys. Org. Chem.* **2011**, *45*, 93–169. (d) Shishlov, N. M. *Russ. Chem. Rev.* **2006**, *75*, 863–884. (e) Rajca, A. *Chem. Rev.* **1994**, *94*, 871–893.
- (4) (a) Rajca, S.; Rajca, A.; Wongsriratanakul, J.; Butler, P.; Choi, S. *J. Am. Chem. Soc.* **2004**, *126*, 6972–6986. (b) Rajca, A.; Wongsriratanakul, J.; Rajca, S. *J. Am. Chem. Soc.* **2004**, *126*, 6608–6626. (c) Rajca, A.; Wongsriratanakul, J.; Rajca, S.; Cerny, R. L. *Chem.–Eur. J.* **2004**, *10*, 3144–3157. (d) Rajca, A.; Lu, K.; Rajca, S. *J. Am. Chem. Soc.* **1997**, *119*, 10335–10345.
- (5) Rajca, A.; Wongsriratanakul, J.; Rajca, S. *Science* **2001**, *294*, 1503–1505.
- (6) (a) Boratyński, P. J.; Pink, M.; Rajca, S.; Rajca, A. *Angew. Chem., Int. Ed.* **2010**, *49*, 5459–5462. (b) Rajca, A.; Shiraishi, K.; Pink, M.; Rajca, S. *J. Am. Chem. Soc.* **2007**, *129*, 7232–7233.
- (7) (a) Rajca, A.; Olankitwanit, A.; Wang, Y.; Boratyński, P. J.; Pink, M.; Rajca, S. *J. Am. Chem. Soc.* **2013**, *135*, 18205–18215. (b) Swager, T. M.; Azzarelli, J. M. *Synfacts* **2014**, *10*, 0142.
- (8) (a) Suzuki, S.; Furai, T.; Kuratsu, M.; Kozaki, M.; Shiomi, D.; Sato, K.; Takui, T.; Okada, K. *J. Am. Chem. Soc.* **2010**, *132*, 15908–15910. (b) Fukuzaki, E.; Nishide, H. *J. Am. Chem. Soc.* **2006**, *128*, 996–1001.
- (9) Davis, R. M.; Sowers, A. L.; DeGraff, W.; Bernardo, M.; Theftford, A.; Krishna, M. C.; Mitchell, J. B. *Free Radical Biol. Med.* **2011**, *51*, 780–790.
- (10) (a) Sowers, M. A.; McCombs, J. R.; Wang, Y.; Paletta, J. T.; Morton, S. W.; Dreaden, E. C.; Boska, M. D.; Ottaviani, M. F.; Hammond, P. T.; Rajca, A.; Johnson, J. A. *Nature Commun.* **2014**, *5*, 5460 DOI: 10.1038/ncomms6460. (b) Rajca, A.; Wang, Y.; Boska, M.; Paletta, J. T.; Olankitwanit, A.; Swanson, M. A.; Mitchell, D. G.; Eaton, S. S.; Eaton, G. R.; Rajca, S. *J. Am. Chem. Soc.* **2012**, *134*, 15724–15727.
- (11) Clore, G. M.; Iwahara, J. *Chem. Rev.* **2009**, *109*, 4108–4139.
- (12) Chiarelli, R.; Novak, M. A.; Rassat, A.; Tholence, J. L. *Nature* **1993**, *363*, 147–149.
- (13) (a) Kinoshita, M. *Magnetism of Stable Organic Radical Crystals, In Handbook of Organic Conductive Molecules and Polymers*, Nalwa, H. S., Ed.; Wiley, 1997; Chapter 15, pp 781–800. (b) Allemann, P.-M.; Khemani, K. C.; Koch, A.; Wudl, F.; Holczner, K.; Donovan, S.; Gruner, G.; Thompson, J. D. *Science* **1991**, *253*, 301–303. (c) Narymbetov, B.; Omerzu, A.; Kabanov, V. V.; Tokumoto, M.; Kobayashi, H.; Mihailovic, D. *Nature* **2000**, *407*, 883–885. (d) Alberola, A.; Less, R. J.; Pask, C. M.; Rawson, J. M.; Palacio, F.; Oliete, P.; Paulsen, C.; Yamaguchi, A.; Farley, R. D.; Murphy, D. M. *Angew. Chem., Int. Ed.* **2003**, *42*, 4782–4785.
- (14) Rajca, A.; Olankitwanit, A.; Rajca, S. *J. Am. Chem. Soc.* **2011**, *133*, 4750–4753.
- (15) Olankitwanit, A.; Rajca, S.; Rajca, A. *J. Am. Chem. Soc.* **2014**, *136*, 14277–14288.

- (16) Barone, V.; Boilleau, C.; Cacelli, I.; Ferretti, A.; Monti, S.; Prampolini, G. *J. Chem. Theory Comput.* **2013**, *9*, 300–307.
- (17) Wenthold, P. G.; Kim, J. B.; Lineberger, W. C. *J. Am. Chem. Soc.* **1997**, *119*, 1354–1359.
- (18) Haider, K. W.; Migirdicyan, E.; Platz, M. S.; Soundararajan, N.; Despres, A. *J. Am. Chem. Soc.* **1990**, *112*, 733–738.
- (19) Pinacolboronates: Sandee, A. J.; Williams, C. K.; Evans, N. R.; Davies, J. E.; Boothby, C. E.; Köhler, A.; Friend, R. H.; Holmes, A. B. *J. Am. Chem. Soc.* **2004**, *126*, 7041–7048.
- (20) Barder, T. E.; Walker, S. D.; Martinelli, J. R.; Buchwald, S. L. *J. Am. Chem. Soc.* **2005**, *127*, 4685–4696.
- (21) Littke, A. F.; Dai, C.; Fu, G. C. *J. Am. Chem. Soc.* **2000**, *122*, 4020–4028.
- (22) At the lower field such as 500 MHz, only broad singlet peak for the aromatic protons, $2H_a$, is found. For the methyl groups, significant broadening for the three singlet peaks, with the outer peaks somewhat more broadened, compared to the center peak, is observed; for more details see: Olankitwanit, A. *Syntheses of Aminyl Diradicals and Nitroxide Tetra- and Octaradicals*; Ph.D. Dissertation; University of Nebraska – Lincoln, Lincoln, NE, October 2014.
- (23) Frisch, M. J. et al. *Gaussian 09*, revision A.01; Gaussian, Inc., Wallingford, CT, 2009.
- (24) Jain, R.; Bally, T.; Rablen, P. R. *J. Org. Chem.* **2009**, *74*, 4017–4023.
- (25) Saielli, G.; Nicolaou, K. C.; Ortiz, A.; Zhang, H.; Bagno, A. *J. Am. Chem. Soc.* **2011**, *133*, 6072–6077.
- (26) Rajca, A.; Boratynski, P. J.; Olankitwanit, A.; Shiraishi, K.; Pink, M.; Rajca, S. *J. Org. Chem.* **2012**, *77*, 2107–2120.
- (27) Rajca, A.; Shiraishi, K.; Boratynski, P. J.; Pink, M.; Miyasaka, M.; Rajca, S. *J. Org. Chem.* **2011**, *76*, 8447–8457.
- (28) (a) Willoughby, P. H.; Jansma, M. J.; Hoye, T. R. *Nat. Protoc.* **2014**, *9*, 643–660. (b) Lodewyk, M. W.; Siebert, M. R.; Tantillo, D. *J. Chem. Rev.* **2012**, *112*, 1839–1862. (c) Barone, G.; Gomez-Paloma, L.; Duca, D.; Silvestri, A.; Riccio, R.; Bifulco, G. *Chem.–Eur. J.* **2002**, *8*, 3233–3239.
- (29) Gennett, T.; Milner, D. F.; Weaver, M. J. *J. Phys. Chem.* **1985**, *89*, 2787–2794.
- (30) Agrawal, A. K.; Jenekhe, S. A. *Chem. Mater.* **1996**, *8*, 579–589.
- (31) Li, Y.; Cao, Y.; Gao, J.; Wang, D.; Yu, G.; Heeger, A. J. *Synth. Met.* **1999**, *99*, 243–248.
- (32) (a) Rajca, A.; Shiraishi, K.; Rajca, S. *Chem. Commun.* **2009**, 4372–4374. (b) Rajca, A.; Takahashi, M.; Pink, M.; Spagnol, G.; Rajca, S. *J. Am. Chem. Soc.* **2007**, *129*, 10159–10170.
- (33) For some samples of **1** and **2**, after initial drop-off in the intensity of the EPR signal due to the reaction with an excess of I_2 , no further change of EPR signal was observed.
- (34) (a) Roberts, J. R.; Ingold, K. U. *J. Am. Chem. Soc.* **1973**, *95*, 3228–3235. (b) Laarhoven, L. J. J.; Mulder, P. *J. Phys. Chem. B* **1997**, *101*, 73–77. (c) Laarhoven, L. J. J.; Mulder, P.; Wayner, D. D. M. *Acc. Chem. Res.* **1999**, *32*, 342–349. (d) Blanksby, S. J.; Ellison, G. B. *Acc. Chem. Res.* **2003**, *36*, 255–263.
- (35) The H-atom abstraction pathway is supported by the presence of small peaks in HR EI-MS of the crude mixtures, corresponding to the monoadducts of 2-MeTHF to **3** or **12**, or **14** (Supporting Information).
- (36) (a) Quantum mechanical tunneling may accelerate hydrogen atom abstraction, e.g., ref 34a. (b) Mendes, J.; Zhou, C.-W.; Curran, H. J. *J. Phys. Chem. A* **2014**, *118*, 1300–1308.
- (37) Ellison, G. B.; Davico, G. E.; Bierbaum, V. M.; DePuy, C. H. *Int. J. Mass Spectrom. Ion Processes* **1996**, *156*, 109–131.
- (38) (a) Soda, T.; Kitagawa, Y.; Onishi, T.; Takano, Y.; Shigeta, Y.; Nagao, H.; Yoshioka, Y.; Yamaguchi, K. *Chem. Phys. Lett.* **2000**, *319*, 223–230. (b) Yamaguchi, K.; Jensen, F.; Dorigo, A.; Houk, K. N. *Chem. Phys. Lett.* **1988**, *149*, 537–542.
- (39) Noodleman, L.; Case, D. A. *Adv. Inorg. Chem.* **1992**, *38*, 423–470.
- (40) Trinquier, G.; Suaud, N.; Malrieu, J.-P. *Chem.–Eur. J.* **2010**, *16*, 8762–8772.
- (41) Quast, H.; Nüdling, W.; Klemm, G.; Kirschfeld, A.; Neuhaus, P.; Sander, W.; Hrovat, D. A.; Borden, W. T. *J. Org. Chem.* **2008**, *73*, 4956–4961.
- (42) Mañeru, D. R.; Pal, A. K.; Moreira, I. P. R.; Datta, S. N.; Illas, F. *J. Chem. Theory Comput.* **2014**, *10*, 335–345.
- (43) Wang, T.; Krylov, A. I. *J. Chem. Phys.* **2005**, *123*, 104304–1–6.
- (44) Barone, V.; Cacelli, I.; Cimino, P.; Ferretti, A.; Monti, S.; Prampolini, G. *J. Phys. Chem. A* **2009**, *113*, 15150–15155.
- (45) Neese, F. *ORCA – an ab initio, Density Functional and Semiempirical program package*, v 2.6; University of Bonn, 2008.
- (46) Sinnecker, S.; Neese, F. *J. Phys. Chem. A* **2006**, *110*, 12267–12275.
- (47) Harris, R. K.; Becker, E. D.; de Menezes, S. M. C.; Goodfellow, R.; Granger, P. *Pure Appl. Chem.* **2001**, *73*, 1795–1818.
- (48) Wishart, D. S.; Bigam, C. G.; Yao, J.; Abildgaard, F.; Dyson, H. J.; Oldfield, E.; Markley, J. L.; Sykes, B. D. *J. Biomolecular NMR* **1995**, *6*, 135–140.
- (49) Spagnol, G.; Rajca, A.; Rajca, S. *J. Org. Chem.* **2007**, *72*, 1867–1869.